

#### **PAPER**

# miRNA induced 3D bioprinted-heterotypic osteochondral interface

To cite this article: Nazmiye Celik et al 2022 Biofabrication 14 044104

View the article online for updates and enhancements.

### You may also like

- Liver-specific microRNAs as biomarkers of nanomaterial-induced liver damage
  Takashi Nagano, Kazuma Higashisaka, Akiyoshi Kunieda et al.
- From reversible to irreversible bistable switches via bifurcations in a gene regulatory network
  Lijie Hao, Zhuoqin Yang, Danhong Shen et al.
- Exploring the influence of microRNA miR-34 on p53 dynamics: a numerical study Nan Liu, , Hongli Yang et al.



## Breath Biopsy® OMNI

The most advanced, complete solution for global breath biomarker analysis









Robust Breath Collection



Reliable Sample Processing & Analysis



In-depth Data Analysis



Specialist Data Interpretation

### Biofabrication



24 January 2022

REVISED

16 May 2022

ACCEPTED FOR PUBLICATION 8 July 2022

PURI ISHED

17 August 2022

#### **PAPER**

### miRNA induced 3D bioprinted-heterotypic osteochondral interface

Nazmiye Celik<sup>1,2</sup>, Myoung Hwan Kim<sup>2,3</sup>, Miji Yeo<sup>1,2</sup>, Fadia Kamal<sup>4</sup>, Daniel J Hayes<sup>2,3,5,\*</sup> and Ibrahim T Ozbolat1

- Department of Engineering Science and Mechanics, Penn State University, University Park, PA 16802, United States of America
- The Huck Institutes of the Life Sciences, Penn State University, University Park, PA 16802, United States of America
- Department of Biomedical Engineering, Penn State University, University Park, PA 16802, United States of America
- Center for Orthopedic Research and Translational Sciences, Department of Orthopedics and Re-Habilitation, Penn State University, Hershey, PA 17033, United States of America
- Materials Research Institute, Penn State University, University Park, PA 16802, United States of America
- Department of Neurosurgery, Penn State University, Hershey, PA 17033, United States of America
- Department of Medical Oncology, Cukurova University, Adana 01330, Turkey
- Authors to whom any correspondence should be addressed.

E-mail: djh195@psu.edu and ito1@psu.edu

Keywords: miRNA, stem cells, spheroids, bioprinting, bone, cartilage

Supplementary material for this article is available online

#### Abstract

The engineering of osteochondral interfaces remains a challenge. MicroRNAs (miRs) have emerged as significant tools to regulate the differentiation and proliferation of osteogenic and chondrogenic formation in the human musculoskeletal system. Here, we describe a novel approach to osteochondral reconstruction based on the three-dimensional (3D) bioprinting of miR-transfected adipose-derived stem cell (ADSC) spheroids to produce a heterotypic interface that addresses the intrinsic limitations of the traditional approach to inducing zonal differentiation via the use of diffusible cytokines. We evaluated the delivery of miR-148b for osteogenic differentiation and the codelivery of miR-140 and miR-21 for the chondrogenic differentiation of ADSC spheroids. Our results demonstrated that miR-transfected ADSC spheroids exhibited upregulated expression of osteogenic and chondrogenic differentiation related gene and protein markers, and enhanced mineralization and cell proliferation compared to spheroids differentiated using a commercially-available differentiation medium. Upon confirmation of the osteogenic and chondrogenic potential of miR-transfected ADSC spheroids, using aspiration-assisted bioprinting, these spheroids were 3D bioprinted into a dual-layer heterotypic osteochondral interface with a stratified arrangement of distinct osteogenic and chondrogenic zones. The proposed approach holds great promise for the biofabrication of stratified tissues, not only for the osteochondral interfaces presented in this work, but also for other composite tissues and tissue interfaces, such as, but not limited to, the bone-tendon-muscle interface and craniofacial tissues.

#### 1. Introduction

Osteochondral lesions (OLs) are widespread injuries localized in articular cartilage and subchondral bone caused by trauma, tumors, or osteoarthritis (OA) [1, 2]. When a lesion occurs, the avascular nature of articular cartilage leads to limited regenerative ability, due to the lack of nutrients, growth factors and progenitor cell supply [3, 4]. Although there has been a significant progress in OL research and lesion-modifying drugs, there are

limited tissue models recapitulating the joint anatomy and physiology to test effective drug and delivery methods, and understand disease progression [5]. Therefore, the development of biomimetic in-vitro models for the osteochondral (OC) interface is important for multiple applications, such as to evaluate the accurate outcome assessment of drug testing and explore the development and progression of different OC-related diseases. In addition, such an interface model can be modified for OL repair and regeneration.

While three-dimensional (3D) bioprinting, particularly scaffold-based bioprinting, has become more accessible with the development of new bioinks and biofabrication approaches [6-9], scaffold-free bioprinting has the advantage of delivering progenitor cells at physiologically-relevant densities along with an intact extracellular matrix (ECM) with their unique similarities to native tissue, to regenerate heterotypic OC interfaces. In our previous research [10], we showed that adipose-derived stem cell (ADSC) spheroids could be considered an effective candidate as building blocks for fabrication of the OC interface. However, use of the traditional differentiation strategy with diffusible cytokines possesses its own intrinsic limitations, such as the need for mixing osteogenic and chondrogenic medium and their potential risk in inhibiting the induction capability of each other, which can reduce the efficacy of heterotypic differentiation and induce ectopic tissue formation. In this regard, MicroRNA (miR) therapeutics holds great potential, as the differentiation of stem cells can be induced without relying on any differentiation medium with diffusible cytokines.

miRs are small ( $\sim$ 18–24 nucleotides) noncoding RNAs targeting mRNA silencing and posttranscriptional regulation of gene expression [11]. They play important roles in cell fates by regulating cellular functions such as cell proliferation, differentiation, and apoptosis [11, 12]. Integrating miRs biology into tissue engineering provides an effective tool to improve the control of cell differentiation and the proliferation functions of tissue engineered grafts [12, 13]. Our previous studies have demonstrated that a single dose of miR-148b mimic effectively drives the osteogenic differentiation of bone marrow-derived stem cells and ADSCs de novo, without other differentiation factors [14, 15]. Recent studies have also revealed that miRs play significant roles in chondrogenesis, cartilage remodeling, and OA development [16-21]. miR-140 is one the most highly expressed miRs, and in recent studies, it has been shown to have tissue specific expression in cartilaginous tissues on zebrafish and mice [22-24]. MiR-140 promotes chondrogenesis by the upregulation of SOX9 and ACAN proteins using an RAS-like proto-oncogene A (RALA) target, which is responsible for the regulation of SOX9 at the protein level [25]. The expression of miR-140 has been demonstrated to modulate chondrogenic differentiation in cartilaginous tissues in mice and zebrafish [23–26], while miR-21 is another widely studied miR and has roles as a regulator of the proliferation of stem and cancer cells [27-29]. miR-21 is known to modulate the duration and magnitude of the extracellular signal-regulated kinase-mitogen-activated protein kinase (ERK-MAPK) signaling by repressing SPRY2 expression during adipogenesis and the osteogenesis of stem cells [30, 31]. ERK-MAPK signaling is the only active pathway for osteogenic, chondrogenic,

and adipogenic lineages during the differentiation of stem cells [30, 31]. In addition, a recent study showed that miR-21 promoted chondrocyte proliferation and cartilage matrix synthesis in rabbit chondrocytes [29]. In this regard, the codelivery of miR-mimics to drive the heterotypic osteogenic and chondrogenic differentiation of progenitor cells, in conjunction with bioprinting, is a potentially effective route to control the development of a spatially-organized OC interface.

In this work, we examined the impact of miR mimic delivery on the differentiation and proliferation of ADSC spheroids, namely miR-148b delivery for osteogenic differentiation and miR-140 and −21 codelivery for chondrogenic differentiation. Upon confirmation of their osteogenic and chondrogenic potential, using aspiration-assisted bioprinting (ABB), miR-transfected spheroids were then 3D bioprinted in double layers in a scaffold-free manner to explore the potency of these spheroids in reconstituting the OC interface. The results demonstrated that the bioprinted OC interface via miR-induced differentiation exhibited distinct osteogenic and chondrogenic layers with better shape retention and higher cell proliferation compared to the OC interfaces generated using the traditional approach relying on diffusible cytokines.

#### 2. Materials and methods

#### 2.1. Cell culture and spheroid fabrication

Human ADSCs (Catalog number: PT-5006, Lonza, Walkersville, MD) were cultured in a basal medium consisting of a 1:1 mixture of HyClone Dulbecco's modified Eagle medium (F12) (Hyclone, Marlborough, MA) supplemented with 20% fetal bovine serum (R&D Systems, Minneapolis, MN), 1% U ml<sup>-1</sup> Penicillin/Streptomycin (Corning, Manassas, VA) at 37 °C with 5% CO<sub>2</sub>. The cell medium was changed every other day. We cultured commercially available human ADSCs and expanded them from passage 1–3, and then used them for our experiments. Cells were received from a single donor. For spheroid fabrication, the ADSCs were harvested with Trypsin and collected by centrifugation at  $1600 \times g$  for 4 min. The ADSCs were reconstituted to  $2.5 \times 10^5$  cells ml<sup>-1</sup>. The cell suspension (200  $\mu$ l) was pipetted into each well of U-bottom 96-well plates (Greiner Bio-One, Monroe, NC) as explained in our previous work [14]. 96-well plates were then incubated in a humidified atmosphere with 5% CO2 at 37 °C overnight for spheroid formation.

# 2.2. Osteogenic and chondrogenic differentiation of ADSC spheroids

Two different differentiation procedures were used for both chondrogenic and osteogenic differentiation. Firstly, spheroids, upon their formation, were cultured in all-in-one ready-to-use human chondrocyte differentiation medium (Catalog number: 411D-250, Cell Applications, San Diego, CA) for chondrogenic differentiation and human osteoblast differentiation medium (Catalog number: 417D-250, Cell Applications, San Diego, CA) for osteogenic differentiation. The medium was changed every three days for four weeks. Secondly, miR mimics were used for both osteogenic and chondrogenic differentiation, according to the protocol reported in our previous work [14]. Custom oligonucleotides (miR-140: 5'-CAG UGG UUU UAC CCU AUG GUA G-3'; miR-21: 5'CAA CAG CAG UCG AUG GGC UGU 3'; miR-148b: 5' UCA GUG CAU CAC AGA ACU UUG U 3') were ordered from Integrated DNA Technologies (Coralville, IA). Invitrogen Lipofectamine RNAiMAX transfection reagent (Thermo Fisher Scientific, Waltham, MA) was used for the transfection and was mixed with miR-148b or miR-(140 + 21)mimics according to the manufacturer's protocol. The ADSCs were transfected with miR-148b-mimic for osteogenic differentiation or miR-(140 + 21)-mimic for chondrogenic differentiation, before being seeded in Opti-MEM medium (Gibco, Carlsbad, CA) in 175 cm<sup>2</sup> cell culture flasks for 24 h. The final concentration of miR-148b and miR-(140 + 21) in the opti-MEM medium was determined to be 200 nM for a volume of 10 ml. The 10 ml solution with the final concentration of 200 nM was transferred to 75 cm<sup>2</sup> cell culture flasks and incubated at 37 °C and 5% CO<sub>2</sub> for 24 h. Transfected cells were collected by trypsinization and formed as spheroids using the protocol explained in section 2.1. Basal medium was used for miR-transfected spheroids and changed every three days for four weeks (see table S1 for medium details). After one, two, three, or four weeks, differentiated spheroids were harvested by firmly pipetting growth medium up and down to dislodge them from 96-well plates.

#### 2.3. Bioprinting of the OC interface

The literature suggests that osteogenic induction takes four weeks [32-34]. Although chondrogenic differentiation takes three weeks, we cultured both osteogenic and chondrogenic groups for four weeks to ensure consistency while combining both types of spheroids and analyzing the bioprinted OC interfaces. After three weeks of differentiation, the fabricated spheroids were harvested by firmly pipetting growth medium up and down to dislodge them from the 96-well plates for bioprinting of the OC interface. A hybrid bioprinting approach encompassing an aspiration-assisted [35] and microvalve bioprinting system [36] were used to develop the OC interface. We used alginate as the support gel since we wanted to remove the gel without any harm to the spheroids and their integrity in assembled interfaces.

Sodium alginate (Sigma Aldrich, St. Louis, MO) was dissolved in ultra-purified water at a

concentration of 0.5% (w/v). Calcium chloride (CaCl<sub>2</sub>, Sigma Aldrich, MO) was dissolved in ultrapurified water at a concentration of 0.4% (w/v). First, a droplet-based bioprinter (jetlab® 4, Micro-Fab Technologies, Plano, TX) was customized for micro-valve bioprinting and placed in a vertical laminar flow cabinet (Air Science Purair VLF36, Fort Myers, FL) for sterility. Specifically, the bioprinter was utilized with a micro-valve dispensing device (The Lee Company; cat. no. INKX0517500A, Westbrook, CT) with a 250 mm nozzle (The Lee Company; cat. no. INZA3100914K, Westbrook, CT). Alginate solution was then printed in a 7 mm circular shape using a pneumatic pressure of 126 kPa, 5 V dwell voltage, 500  $\mu$ s dwell time, 1  $\mu$ s rise/fall time, 0 V echo voltage, 20  $\mu$ s echo time, and 100 Hz frequency. Next, the printed structure was crosslinked via aerosol crosslinking using CaCl2 for 10 min. Second, two different groups of spheroids, either differentiated using osteogenic and chondrogenic differentiation medium, or differentiated using miR-148b and miR-(140 + 21) mimics, were deposited via ABB in two layers (first layer: 16 chondrogenic spheroids; second layer: 9 osteogenic spheroids) onto the previously printed alginate support. Third, following ABB, alginate was micro-valve printed again to lay over the bioprinted spheroids in order to fix their position. The bioprinted structure was then immersed into CaCl<sub>2</sub> solution for 1 min for complete crosslinking and then washed twice using PBS. The bioprinted OC interfaces were cultured in a medium consisting of chondrogenic and osteogenic medium mixed in 1:1 ratio for the differentiation medium group, or in basal medium for the miR transfection group. The medium was changed every other day (see table S1 for medium details). After a one week culture in the medium, the spheroids fused completely, and the alginate was de-crosslinked using a 4% sodium citrate (Sigma Aldrich, MO) solution (dissolved in ultra-purified water at a concentration of 0.4% w/v), leaving the OC interface behind [37].

# 2.4. Gene expression using quantitative real-time polymerase chain reaction (qRT-PCR)

To evaluate osteogenic and chondrogenic gene expression profiles using qRT-PCR, RNA was isolated from spheroids of miR-148b transfected, miR-(140 + 21) transfected, osteogenic control, chondrogenic control, and negative control groups, using TRIzol reagent (Life Technologies, CA) and PureLink RNA Mini Kit (Thermo Fisher Scientific, Waltham, MA) according to the manufacturer's protocol at Weeks 1, 2, 3, and 4. Also, 3D bioprinted samples from differentiation medium and miR-transfected groups were homogenized in TRIzol reagent, followed by using the PureLink RNA Mini Kit according to the manufacturer's protocol at Week 4. The RNA concentration of each sample was measured using

**Table 1.** Primers of the genes used in the qRT-PCR study.

Gene	Forward primer	Reverse primer
COL1	ATG ACT ATG AGT ATG GGG AAG CA	TGG GTC CCT CTG TTA CAC TTT
RUNX2	GGT TAA TCT CCG CAG GTC ACT	CAC TGT GCT GAA GAG GCT GTT
BSP	AAC GAA GAA AGC GAA GCA GAA	TCT GCC TCT GTG CTG TTG GT
BMP4	TAG CAA GAG TGC CGT CAT TCC	GCG CTC AGG ATA CTC AAG ACC
OSTERIX	CCT CTG CGG GAC TCA ACA AC	AGC CCA TTA GTG CTT GTA AAG G
SOX9	AGC GAA CGC ACA TCA AGA C	CTG TAG GCG ATC TGT TGG GG
COL2A1	CCA GAT GAC CTT CCT ACG CC	TTC AGG GCA GTG TAC GTG AAC
COL1A1	GGA GGA GAG TCA GGA AGG	TCA GCA ACA CAG TTA CAC AA
ACAN	TCC CCT GCT ATT TCA TCG AC	CCA GCA GCA CTA CCT CCT TC
GAPDH	CAC ATG GCC TCC AAG GAG TA	GTA CAT GAC AAG GTG CGG CT

a Nanodrop (Thermo Fisher Scientific, Waltham, MA). AccuPower® CycleScript RT PreMix (BION-EER, Korea) was used for the conversion of RNA to cDNA following the manufacturer's instructions. Gene expression was analyzed quantitatively with PowerUp™ SYBR™ Green Master Mix (Thermo Fisher Scientific, Waltham, MA) using a Quant-Studio 3 PCR system (Thermo Fisher Scientific, Waltham, MA). The osteogenic genes tested included collagen type-1 (COL-1), runt-related transcription factor-2 (RUNX2), bone sialoprotein (BSP), bone morphogenetic protein-4 (BMP-4), and transcription factor Sp7 (OSTERIX). The chondrogenic genes tested included SOX9 (SRY-Box Transcription Factor 9), COL2A1 (alpha-1 chain of type II collagen), COL1A1 (alpha-1 chain of type I collagen), and ACAN (Aggrecan). All primers are listed in table 1. All genes were normalized to the expression of a glyceraldehyde three-phosphate dehydrogenase gene, and the  $2^{-\Delta\Delta CT}$  method was used to calculate gene expression levels relative to the negative controls.

#### 2.5. Histology

Single spheroids for all groups were fixed in 4% paraformal dehyde for 3 h at room temperature at Weeks 1, 2, 3, and 4 of differentiation. Bioprinted OC interface samples were also fixed in 4% paraformal dehyde for 3 h at room temperature at Week 4 of differentiation. The samples gradually dehydrated in alcohol and were embedded in paraffin blocks using a Leica TP 1020 automatic tissue processor (Leica, Buffalo Grove, IL). Then, samples were cut into 10  $\mu$ m sections with a Shandon Finesse® Paraffin microtome (Thermo Electron Corporation, Waltham, MA) and placed onto positively charged slides. The collected sections were used for all chemical and immunofluorescence staining experiments.

#### 2.6. Hematoxylin and eosin (H&E) staining

Sectioned samples of single spheroids and bioprinted tissues were stained with H&E using a Leica Autostainer ST5010 XL (Leica, Germany) based on the manufacturer's protocol. After the staining process, sections were mounted using a Xylene Substitute Mountant (Thermo Fisher Scientific, Waltham, MA)

and kept at room temperature to dry overnight. The stained samples were imaged using an EVOS fluorescence microscope (Invitrogen, Waltham, MA).

#### 2.7. Toluidine Blue O and Alizarin Red S staining

The sections were dewaxed using the Leica Autostainer and underwent Toluidine Blue O and Alizarin Red S staining according to standard protocols. Briefly, for Toluidine blue O staining, the sections were incubated in a Toluidine blue solution (0.1% in DI water, Sigma Aldrich) at room temperature for 2 min. The dye was then removed, and samples were washed twice with deionized water. The samples were sequentially dehydrated with 95 and 100% alcohol and cleared with Xylene. Then, coverslips were mounted to the slides using the Xylene Substitute Mountant.

For Alizarin Red S staining, sections were incubated with Alizarin Red solution (EMD Millipore Corp., Billerica, MA) at room temperature for 40 min. Excess dye was removed and washed four times with DI water. After dehydration with ascending alcohol and clearing with Xylene, coverslips were mounted to the slides using the Xylene Substitute Mountant. The differentiated cells containing mineral deposits were imaged as stained bright red using the EVOS fluorescence microscope.

#### 2.8. PicoGreen cell proliferation assay

The DNA content of each sample was measured by a DNA quantitation assay using a A Quantit PicoGreen ds-DNA Assay Kit (Molecular Probes Inc., Eugene, OR). First, a standard curve was made using two, four, six, eight, and ten spheroids (with  $2.5 \times 10^5$  cell/spheroid). The number of repeats was five. The standard curve was made using the standard protocol for PicoGreen studies.

For sample preparation, ten spheroids per group were used at Weeks 1, 2, 3, or 4. Proteinase K of 0.4 ml (Sigma Aldrich) at a final concentration of 0.5 mg ml<sup>-1</sup> was first added to each well, and plates were incubated at 56 °C overnight for the enzymatic lysis of cells and DNA release. Aliquots (50  $\mu$ l) were mixed with equal volumes of 0.1 g ml<sup>-1</sup> Pico-Green® dye solution (Invitrogen) in 96-well plates.

Samples were then excited at 480 nm with an emission wavelength of 520 nm using a plate reader (Power-WaveX, BioTek, Winooski, VT). The otal DNA concentration was compared to a standard curve generated from serial dilutions of ADSCs to calculate the number of cells in each well. Samples prepared without cells served as blank controls.

#### 2.9. Biochemical assays

To check the quantity of sulfated glycosaminoglycan (sGAG) secretion, spheroids transfected by miR-(140 + 21) and spheroids differentiated using the chondrogenic differentiation medium were examined using a Glycosaminoglycans Assay Kit (Chondrex, Inc., Redmond, WA). For each group, ten spheroids were collected and rinsed with PBS weekly for four weeks. Proteinase K of 0.4 ml (Sigma Aldrich) at a final concentration of 0.5 mg ml<sup>-1</sup> was first added to each Eppendorf tube with ten spheroids and then incubated at 56 °C overnight for the enzymatic lysis of cells and DNA release. After adding 1, 9 dimethylmethlyene blue solution for 3 min as per the manufacturer's instructions, the absorbance was measured at 525 nm using the microplate reader (PowerWaveX). The sGAG content from each sample was normalized to the dsDNA content.

To check the quantity of alkaline phosphatase (ALP) secretion, spheroids transfected by miR-148b and spheroids differentiated using osteogenic differentiation medium were used. ALP activity assay was conducted using an ALP assay kit (K412-500; BioVision, Inc., Mountain View, CA) according to the manufacturer's instructions. Ten spheroids per sample were resuspended in an assay buffer and subsequently centrifuged at  $13\,000 \times g$  for  $3\,\text{min}$  at  $4\,^{\circ}\text{C}$  to remove any insoluble material. The supernatant was mixed with p-nitrophenyl phosphate (pNPP) substrate and then incubated at  $25\,^{\circ}\text{C}$  for 60 min. The optical density of the resultant pNPP was determined at 405 nm using the microplate reader (PowerWaveX).

#### 2.10. Mineralization staining

The hydroxyapatite deposition of bioprinted OC interfaces were assessed after a week after bioprinting using the Osteoimage<sup>™</sup> Mineralization Assay (Lonza Walkersville, MD). Sectioned samples were washed three times with Osteoimage<sup>™</sup> wash buffer at room temperature and then incubated with 2 ml of staining reagent for 30 min in the dark at room temperature. The samples were then imaged using a Zeiss LSM 880 Airyscan confocal microscope (Zeiss, Oberkochen, Germany).

#### 2.11. Immunohistochemistry stud

Sectioned samples were permeabilized in 0.2% Triton X-100 for 10 min. Next, samples were washed in 1X PBS and then blocked with 2.5% normal goat serum (NGS) for 60 min at room temperature. To visualize osteogenic tissue formation, samples were

incubated with mouse anti-RUNX2 primary antibody (1:20 in 2.5% NGS; Cat. No: ab76956; Abcam, Cambridge, UK) and rabbit anti-Sp7 OSTERIX (1:150 in 2.5% NGS; Cat. No: ab209484, Abcam) overnight, washed three times with DPBS and incubated with goat anti-mouse IgG (H + L)-Alexa Fluor 488 secondary antibody (1:200 in PBS; Cat. No: A11017; Invitrogen), and goat anti-rabbit IgG (H + L)-Alexa Fluor 647 secondary antibody (1:200 in PBS; Cat. No: A21245; Invitrogen) for 3 h. The stained samples were then washed three times with dulbecco's phosphate-buffered saline (DPBS), mounted with Prolong<sup>TM</sup> Gold antifade reagent with 4',6-diamidino-2-phenylindole (DAPI, Invitrogen, molecular probes), and imaged using the Zeiss confocal microscope.

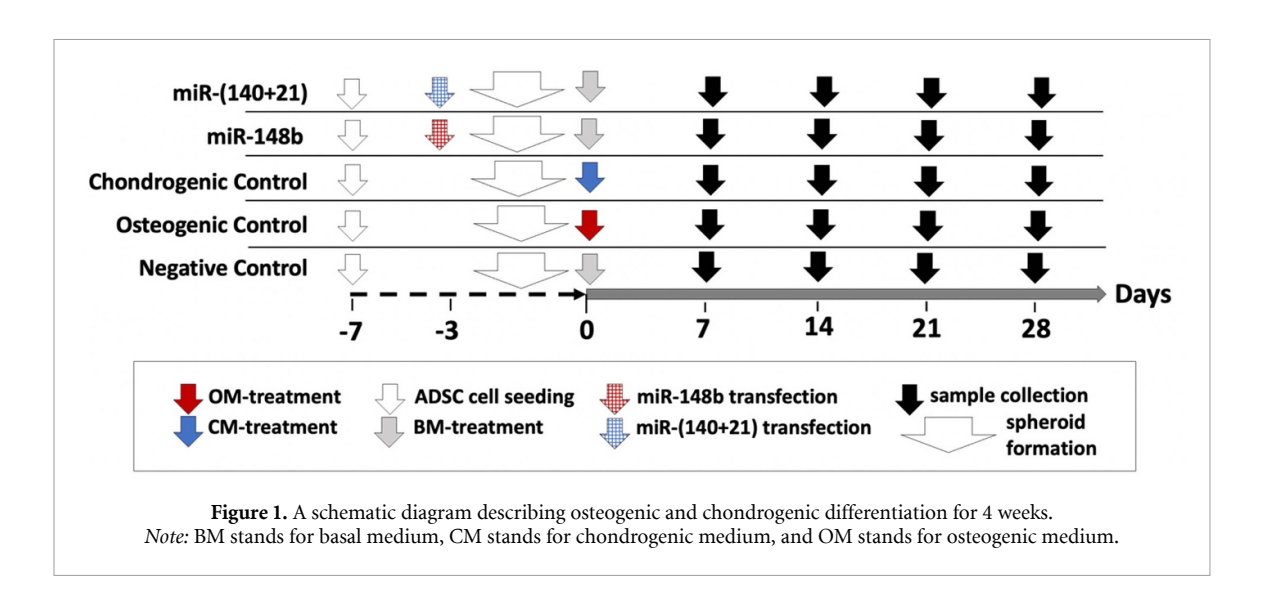
To visualize chondrogenic tissue formation, samples were incubated with mouse anti-Aggrecan (BC-3) primary antibody (1:50 in 2.5% NGS; Cat. No:MA3-16888; ThermoFisher Scientific) and rabbit anti-Col-II (1:100 in 2.5% NGS; Cat. No: ab34712, Abcam, Cambridge, UK) overnight, washed three times with DPBS and incubated with goat anti-mouse Alexa Fluor IgG (H + L)-488 secondary antibody (1:200 in 2.5% NGS; Cat. No: A11017; Invitrogen), and goat anti-rabbit IgG (H + L)-Alexa Fluor 647 secondary antibody (1:200 in 2.5% NGS; Cat. No: A21245; Invitrogen) for 3 h. the stained samples were then washed three times with DPBS, mounted with Prolong<sup>TM</sup> Gold antifade reagent with DAPI (Invitrogen, molecular probes), and imaged using the Zeiss confocal microscope.

#### 2.12. Statistical analysis

All data were presented as mean  $\pm$  standard deviation. Multiple comparisons were analyzed using one-way analysis of variance followed by Post hoc Tukey's multiple-comparison test to determine the individual differences among the groups. Differences were considered significant at  $p^* < 0.05$ ,  $p^{**} < 0.01$ ,  $p^{***} < 0.001$ , and  $p^{****} < 0.0001$ . All statistical analysis was performed using Prism Software (GraphPad Software Inc., La Jolla, CA). We used n=3 samples for experiments related to qRT-PCR and at least three replicates per sample for each of the biological experiments (staining and imaging). We also used n=5 replicates for PicoGreen, sGAG, and ALP activity assays.

#### 3. Results

In our initial study, the chondrogenic induction potential of two miR-mimics, namely miR-21 and miR-140, were explored for ADSCs grown on tissue culture plates in 2D using immunostaining and qRT-PCR, where expression levels of SOX9, COL-1, COL2A1, and ACAN were determined (figure S1). The data suggest that increased chondrogenic genes were observed when ADSCs were co-delivered with



miR-21 and -140 compared to their individual delivery. Increased Aggrecan and Coll-2 expression were also found, providing further evidence that using the co-delivery approach was more effective for promoting chondrogenic differentiation than the use of miR-21 or miR-140 delivery alone. Based on these preliminary results, for the rest of this study, the co-delivery of miR-140 and miR-21 was used for chondrogenic differentiation of ADSCs, and spheroids were formed using miR-(140 + 21) transfected ADSCs to examine the potential for ADSC commitment into a chondrogenic lineage. For comparison with the traditional approach, ADSC spheroids were also treated with a commercially available differentiation medium as a chondrogenic (positive) control group. ADSC spheroids treated with basal medium were used as the negative control group. Figure 1 demonstrates different treatment groups and respective timeline for the differentiation process.

Expressions of chondrogenic protein markers, Aggrecan and Coll2, were examined weekly using immunofluorescent staining (figures 2(a) and 82-85). A large cluster of Aggrecan expression was observed in both spheroids created using miR-(140+21) transfected ADSCs and spheroids treated with chondrogenic differentiation medium. Spheroids that were formed using miR-(140+21) transfected ADSCs exhibited the strongest fluorescent intensity of Coll2 at Week 3. However, a distinguishable Coll2 expression was observed during four weeks in both groups, particularly after Week 2.

Differential gene expression was also quantified for spheroids treated with miR-(140 + 21) transfection compared to spheroids treated with chondrogenic differentiation medium and basal medium for four weeks. SOX9, COL2A1, COL1A1, and ACAN genes were used to assess chondrogenic differentiation. While spheroids transfected with miR-(140 + 21) showed a significantly increased expression of COL1A1 at Week 1 compared to that

of spheroids in the chondrogenic control group, in the chondrogenic control group, expression levels of SOX9, COL2A1, and ACAN were similar (figure 2(b)). At Week 2, spheroids treated with the chondrogenic differentiation medium exhibited a sharp drop in expressions of SOX9, COL2A1, and ACAN. However, the transfected group showed significantly increased expression levels of SOX9, COL2A1 and ACAN at Week 2. While no significant differences were observed between groups for COL1A1 and ACAN expressions, the transfected group showed significantly increased expression of SOX9 and COL2A1 at Week 3. During the last week of differentiation, no significant difference was observed for the expression levels of genes, except ACAN, which was higher for the transfected group.

The morphology of chondrogenic spheroids (differentiated using miR-(140 + 21) transfection and chondrogenic differentiation medium) and spheroids treated with basal medium as the negative control were evaluated using H&E staining at Weeks 1, 2, 3, and 4. In H&E images, no distinct difference in morphology and color was observed between the miR-(140 + 21) transfected and chondrogenic control group over four weeks. These chondrogenic spheroids were stained less intensely indicating a lower density of matrix deposition at Weeks 3 and 4 (figure 3(a)).

Glycosaminoglycan (GAG) content was evaluated for spheroids transfected by miR-(140 + 21) and compared to spheroids in positive and negative control groups at Weeks 1, 2, 3, and 4. Both the miR-(140 + 21) and positive control groups demonstrated an increasing trend in GAG expression over time. Although miR-(140 + 21) transfected spheroids showed a greater GAG content with no significant difference compared to spheroids in the positive control group (with an  $\sim$ 1.1-fold increase) at Week 3, both groups showed a similar GAG content, which was  $\sim$ 2.4 folds greater than the spheroids in the negative control group at Week 4 (figure 3(b1)). DNA content

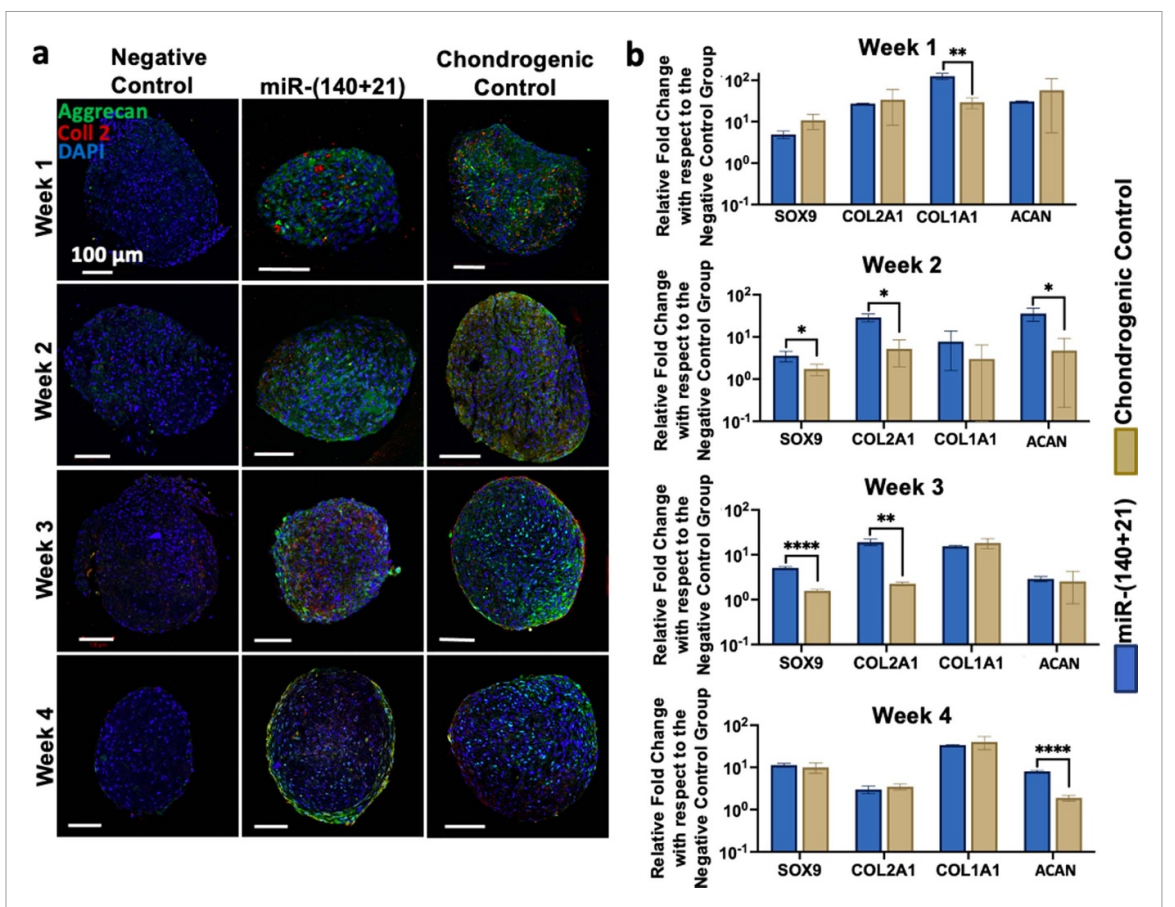


**Figure 2.** Chondrogenic differentiation of ADSC spheroids. (a) Immunostaining images and (b) SOX9, COL2A1, COL1A1, and ACAN expression of spheroids for the negative control, miR-(140 + 21) transfected, and chondrogenic control groups at Weeks 1, 2, 3, and 4. Scale bars in insets correspond to 100  $\mu$ m (n = 3;  $p^* < 0.05$ ;  $p^{**} < 0.01$ ;  $p^{****} < 0.0001$ ).

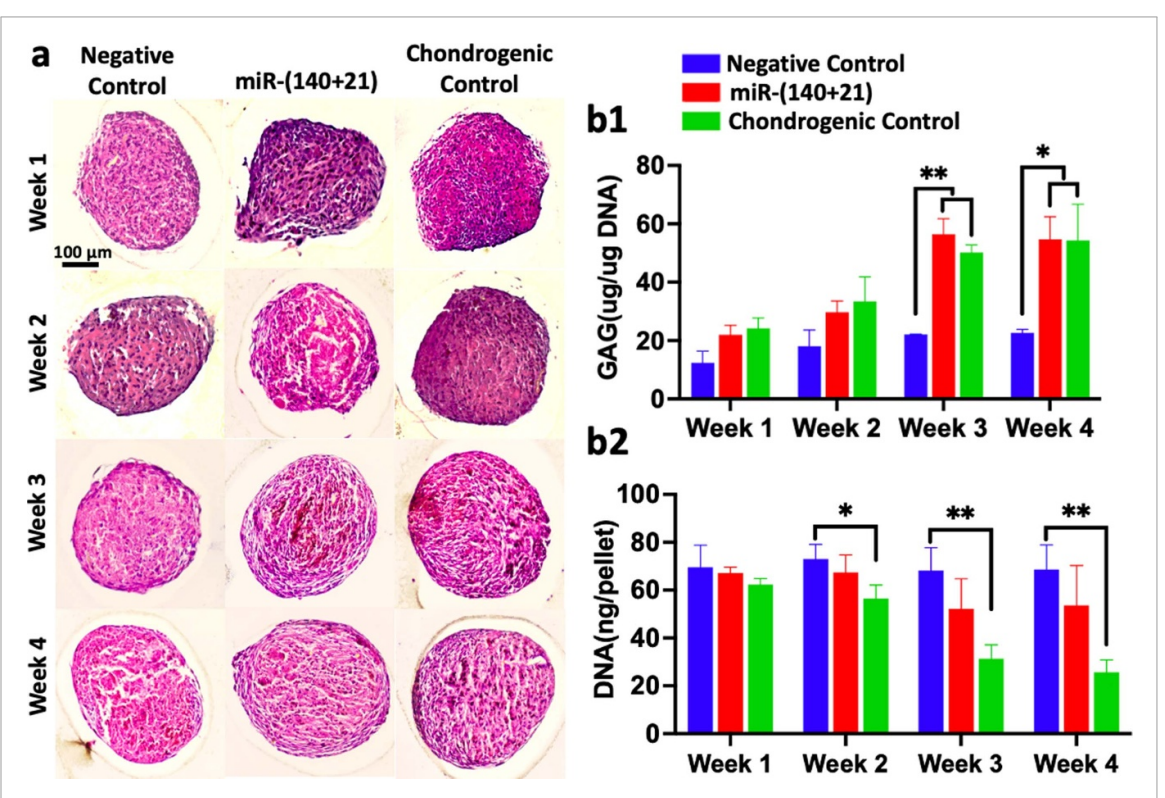


**Figure 3.** Chondrogenic spheroids: (a) H&E images, (b1) sGAG, and (b2) total DNA content of single spheroids from the negative control, miR-(140 + 21) transfected, and chondrogenic control groups at Weeks 1, 2, 3, and 4 (n = 3;  $p^* < 0.05$ ;  $p^{**} < 0.01$ ).

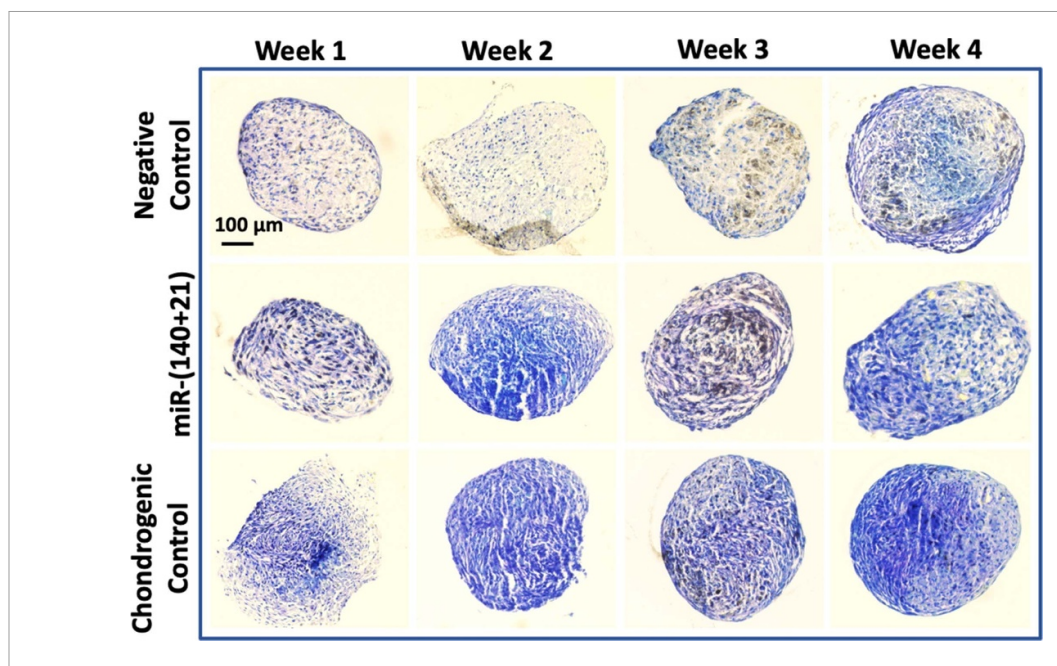


Figure 4. Toluidine Blue staining of chondrogenic spheroids at Week 1, 2, 3, and 4.

was quantified in order to investigate the proliferation ability of the spheroids. Although the negative control group had stable proliferation over time, spheroids in the positive control group showed decreased cell proliferation, which correlated with increased differentiation marker expressions (figure 3(b2)). Interestingly, the spheroids transfected with miR-(140 + 21) had a higher DNA content compared to spheroids treated with chondrogenic differentiation medium, even if they showed similar patterns of differentiation marker expression over time.

In order to further confirm the chondrogenic differentiation of spheroids, Toluidine Blue staining was performed as an end point measure. Toluidine Blue staining of spheroids in both miR-(140 + 21) and positive control groups showed intense staining, demonstrating a higher level of sGAG deposition, while the negative control group exhibited a limited amount of sGAG secreted during the four week differentiation process (figure 4).

Upon confirmation of the chondrogenic potential of miR-(140 + 21) transfected spheroids, ADSC spheroids were also transfected by miR-148b in order to induce osteogenic differentiation. For comparison purposes, ADSC spheroids treated with the commercially available differentiation medium were used as an osteogenic (positive) control group. ADSC spheroids treated with basal medium were used as a negative control group.

As with chondrogenic spheroids, immunofluorescent imaging was used to evaluate the expression of the osteogenic markers, RUNX2 and OSTERIX, for osteogenic spheroids at Weeks 1, 2, 3, and 4 (figures 5(a) and S6–S9). Large clusters of RUNX2 expression were observed for spheroids treated with miR-148b during the first two weeks of differentiation. Spheroids treated with the osteogenic differentiation medium also exhibited RUNX2 expression, particularly at Weeks 3 and 4. In addition, miR-148b transfected spheroids showed distinct OSTERIX expression at Weeks 3 and 4 and exhibited the strongest fluorescent intensity of OSTERIX at Week 4 compared to the osteogenic control group.

qRT-PCR was used to quantify the gene expression profiles of spheroids from all groups weekly. Col-1, RUNX2, BSP, BMP-4, and OSTERIX were used as markers for osteogenesis (figure 5(b)). While no significant difference was observed for the expression levels of osteogenic markers except for RUNX2 at Week 1, Col-1, BSP, BMP-4, and OSTERIX were expressed significantly for the miR-148b transfected group compared to the osteogenic control group at Week 2. At Week 3, the osteogenic control group showed increased fold-change in COL-1 and BMP-4 expressions. There was a significant increase in the expression levels of RUNX2, BMP-4 and OSTERIX in the miR-148b transfected group at Week 4 as compared to those at Week 3 with a fold-increase of  $\sim$ 3.3,  $\sim$ 1.3, and  $\sim$ 2.4, respectively.

The morphology of osteogenic spheroids (differentiated using miR-148b transfection and osteogenic differentiation medium), and spheroids treated with basal medium as the negative control, were evaluated using H&E staining at Weeks 1, 2, 3, and 4. In figure 6(a), osteogenic spheroids differentiated using miR-148b transfection or osteogenic differentiation medium showed an increased bone matrix deposition over time. However, miR-148b transfected spheroids were stained for a darker color, indicating a higher density of matrix deposition at

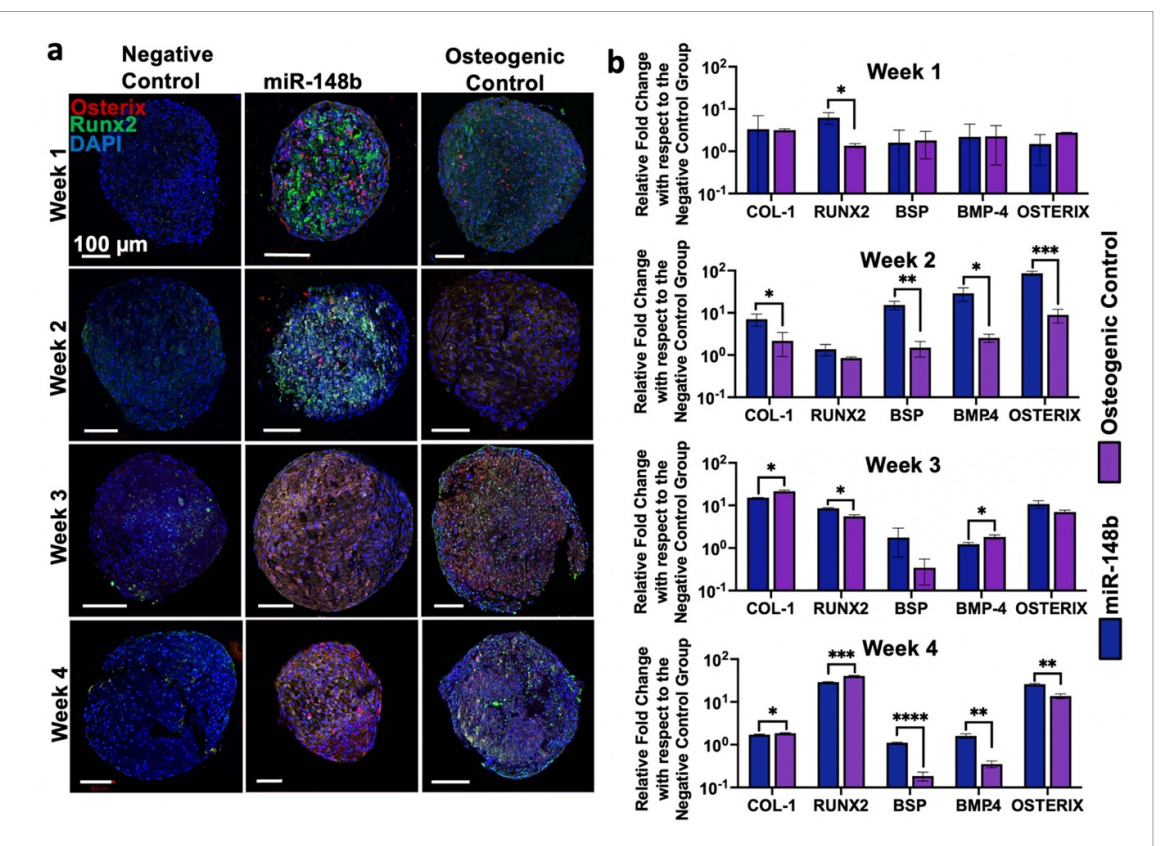


**Figure 5.** Osteogenic differentiation of ADSC spheroids: (a) immunostaining images and (b) COL-1, RUNX2, BSP, BMP-4, and OSTERIX expression of spheroids for the negative control, miR-148b transfected, and osteogenic control groups at Weeks 1, 2, 3, and 4. Scale bars in insets correspond to 100  $\mu$ m (n = 3;  $p^* < 0.05$ ;  $p^{***} < 0.01$ ;  $p^{****} < 0.001$ ;  $p^{****} < 0.0001$ ).

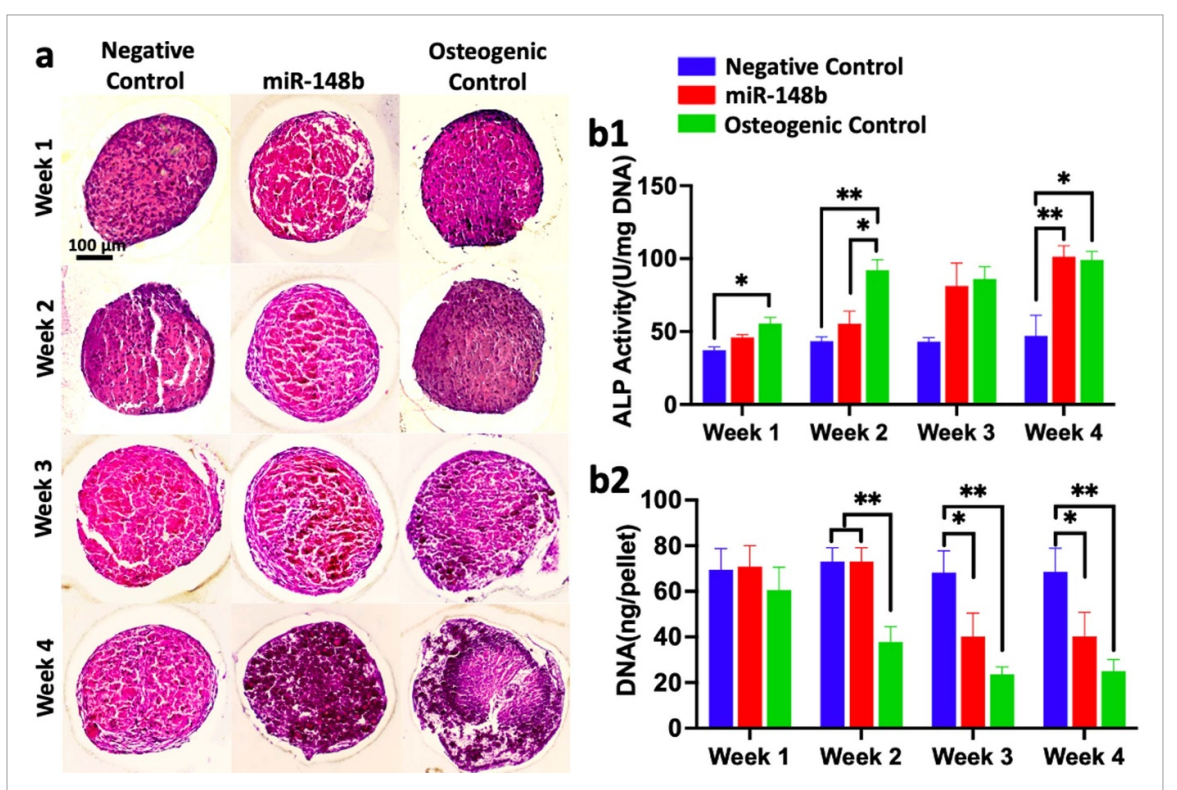


**Figure 6.** Morphological analysis, ALP activity, and cell proliferation of osteogenic spheroids; (a) H&E images, (b1) ALP activity, and (b2) DNA content of single spheroids from the negative control, miR-148b transfected, and osteogenic control groups at Week 1, 2, 3, and 4 (n = 3;  $p^* < 0.05$ ;  $p^{**} < 0.01$ ).

N Celik et al

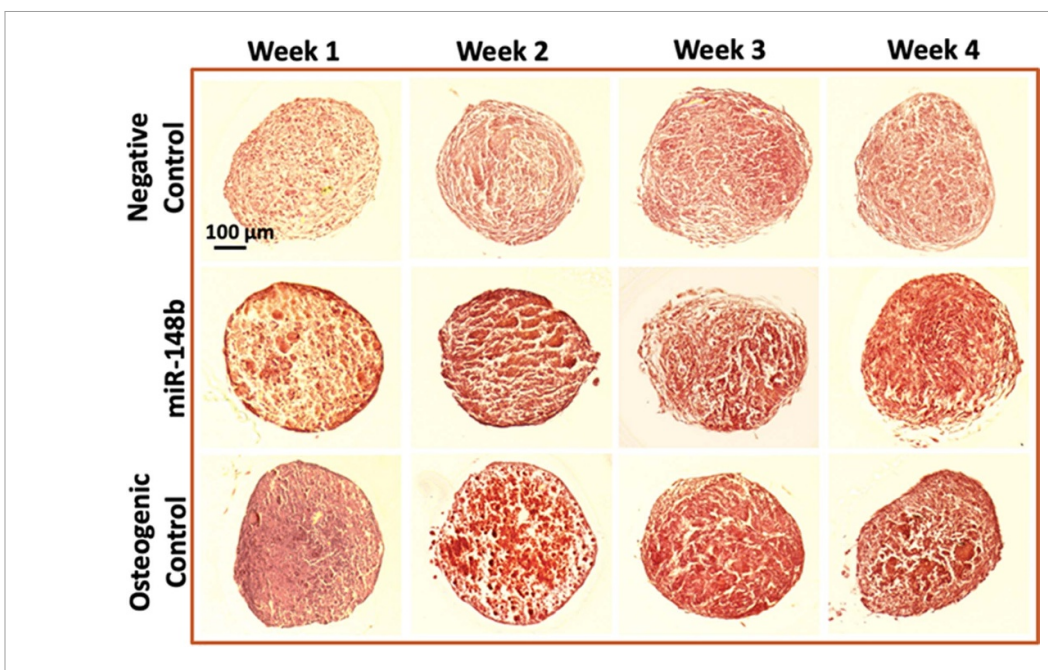


Figure 7. Alizarin red staining of osteogenic spheroids at Week 1, 2, 3, and 4.

Week 4 compared to other groups. ALP content was evaluated for spheroids from all groups at Weeks 1, 2, 3, and 4. Spheroids treated with osteogenic differentiation medium showed significantly greater ALP activity than miR-148b transfected spheroids at Week 2 (figure 6(b1)). However, transfected spheroids increased their ALP activity over time and were similar to spheroids treated with osteogenic differentiation medium and ~2.2-fold higher compared to the spheroids treated with basal medium at Week 4 (figure 6(b1)). Similar to chondrogenic spheroids, the DNA content of osteogenic spheroids was quantified in order to investigate cell proliferation. Although the negative control group had stable proliferation over time, spheroids treated with osteogenic differentiation medium showed decreased cell proliferation, which correlated with increased differentiation marker expression (figure 6(b2)). Spheroids transfected by miR-148b had a higher DNA content compared to spheroids treated with osteogenic differentiation medium, even if they showed similar patterns of differentiation marker expression over time.

In order to further confirm the osteogenic differentiation of spheroids, Alizarin Red staining was performed as an end point measure. Both spheroids, transfected by miR-148b and treated with osteogenic differentiation medium, exhibited an increased signal for Alizarin Red, indicating the abundance of calcification, as compared to spheroids in the negative control group during the four week differentiation process (figure 7).

Upon confirmation of miR-transfected chondrogenic and osteogenic spheroids, OC interfaces were

bioprinted using two different groups, the differentiation medium and miR transfection groups, following the experimental plan demonstrated in figure 8. Osteogenic and chondrogenic ADSCs were formed into spheroids, cultured for three weeks, and then 3D bioprinted and stacked in bilayers to recapitulate the organization of the OC interface.

As shown in figure 9, a multi-stage procedure was followed to build the OC interface. First, microvalve bioprinting was used to deposit a layer of alginate as a support layer. Next, CaCl<sub>2</sub> was introduced via aerosol crosslinking and then AAB was used to bioprint spheroids. 16 and 9 chondrogenic and osteogenic spheroids were bioprinted for the chondrogenic and osteogenic layers, respectively. Upon depositing the spheroids, the bioprinted constructs were then overlaid with alginate in order to secure the spheroids in place. The bioprinted constructs were maintained in alginate support for seven days in order to facilitate the fusion of the spheroids. The support was then dissolved and cross-sections of the bioprinted OC interfaces were analyzed at Week 4.

In order to confirm osteogenic and chondrogenic differentiation of the OC interfaces, Toluidine Blue, Alizarin Red, H&E, and OsteoImage staining were performed along with the immunofluorescent staining for Coll2 and OSTERIX. Toluidine blue staining showed a significant proteoglycan in the chondrogenic zone for both approaches (figure 10). Alizarin Red staining showed a large cluster of dark red staining for calcium deposits, which were indicators of mature osteocytes in the osteogenic zone for both approaches. The cross-sections of chondrogenic and

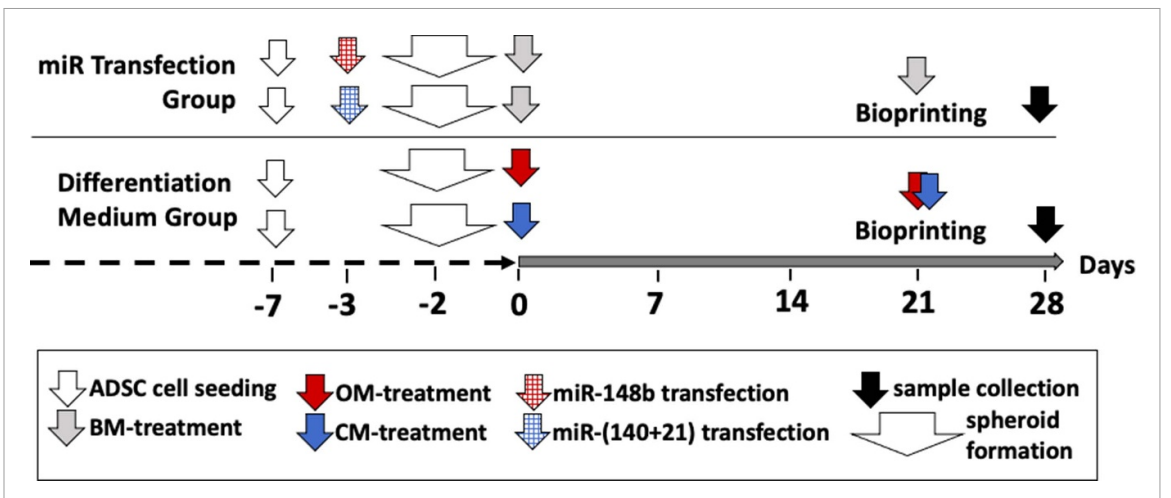


**Figure 8.** A schematic diagram describing the timeline for the bioprinting process for fabrication of the osteochondral interface using osteogenic and chondrogenic spheroids differentiated via two different approaches.

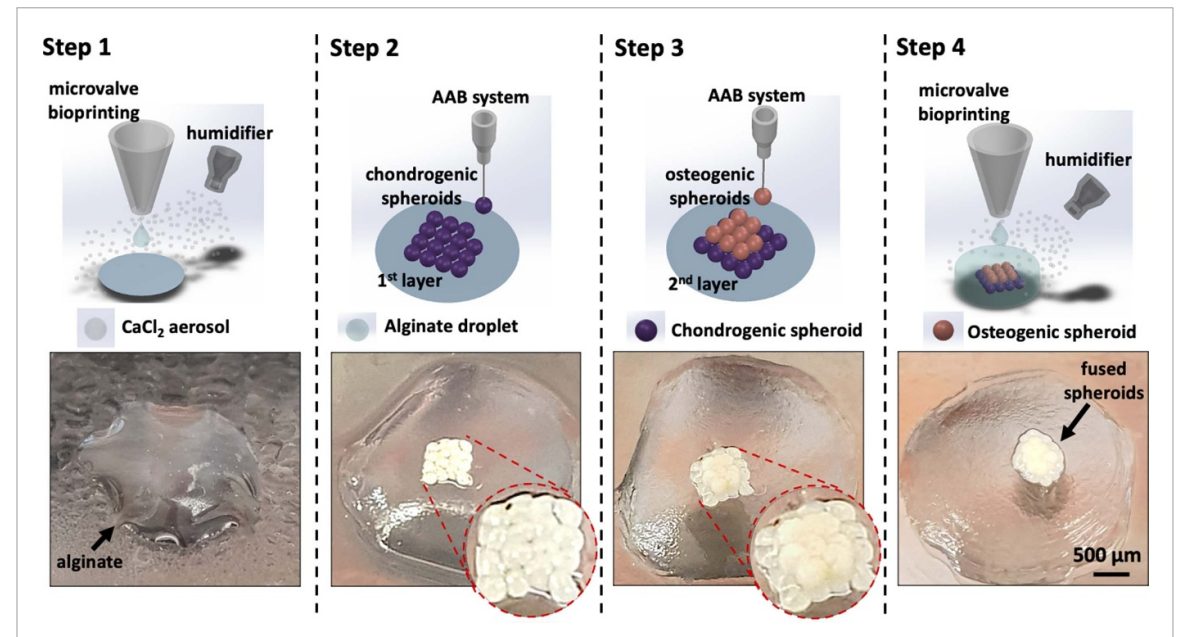


**Figure 9.** A schematic showing the 3D bioprinting of the OC interface using osteogenic and chondrogenic spheroids and the corresponding images demonstrating steps involved in the physical process.

osteogenic layers for both approaches exhibited wellfused spheroids with high-density ECM deposition in the osteogenic zone at Week 4 as shown in H&E images. The miR-transfected group maintained the bilayer morphology better than those formed using spheroids treated with the differentiation medium. OsteoImage mineralization assay was performed to assess mineralization in the bioprinted tissues. A large cluster of mineralization was observed, demonstrating hydroxyapatite formation on the osteogenic zone for both approaches. Concordant with Alizarin Red and OsteoImage staining, OSTERIX staining was more prominent in the osteogenic zone for both approaches with visible florescence clusters at Week 4 (figure 10(b)). In addition, concordant with Toluidine Blue staining, Coll2 was strongly expressed in the

chondrogenic zone for both approaches with visible florescence clusters at Week 4 (figure 10(b)).

Further evidence of osteogenic and chondrogenic differentiation of the OC interface was confirmed by qRT-PCR for both approaches at Week 4 (figure 10(c)). To assess the osteogenic differentiation of bioprinted tissues, COL-1, RUNX2, BSP, BMP-4, and OSTERIX genes were used, while SOX9, COL2A1, COL1A1, and ACAN genes were used to confirm chondrogenic differentiation. the bioprinted tissues formed by spheroids transfected by miR-148b and miR-(140 + 21) exhibited higher expression levels for BSP and OSTERIX than the constructs formed by spheroids treated with the osteogenic and chondrogenic differentiation medium (figure 10(c)). In contrast, the bioprinted

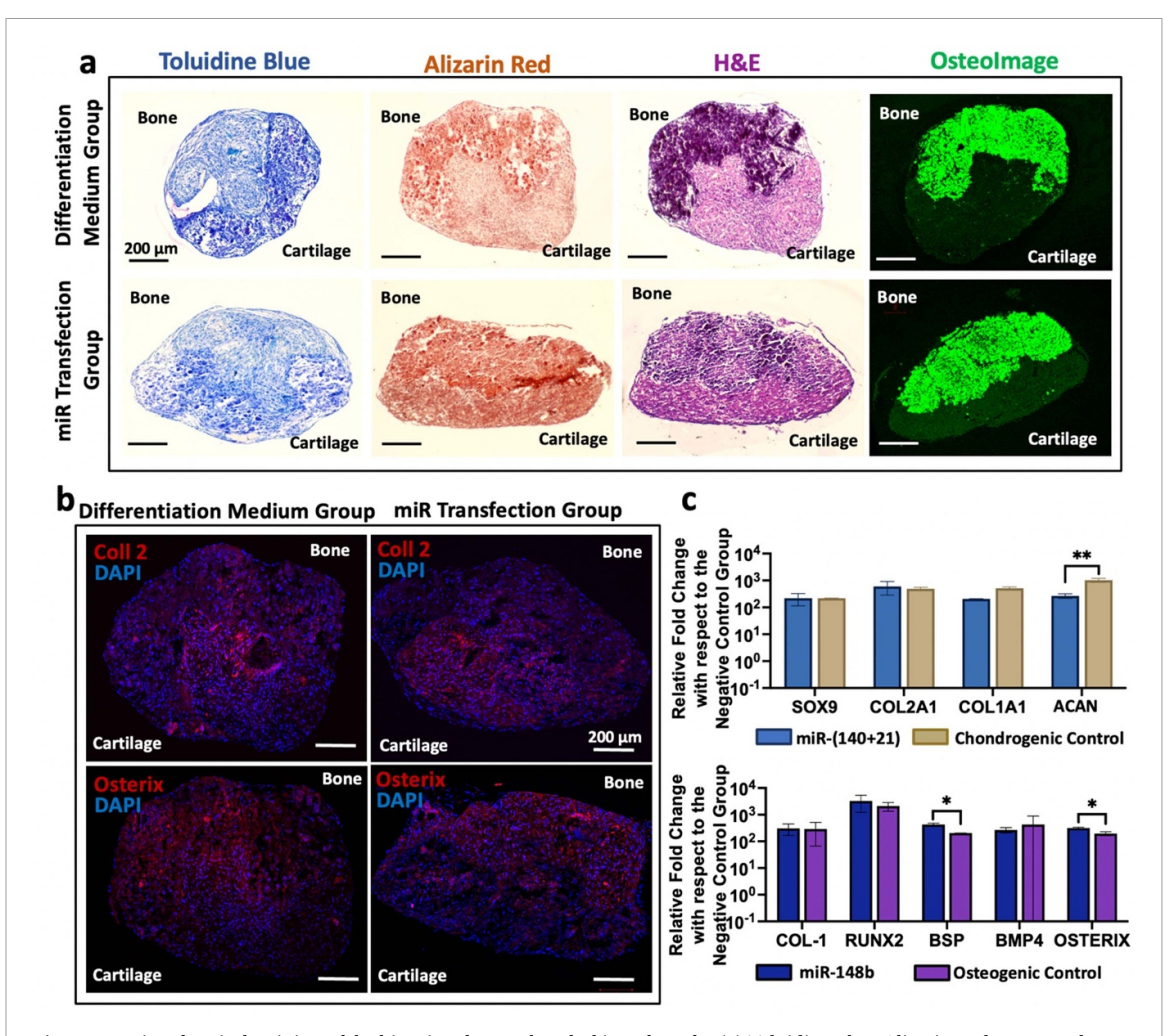


**Figure 10.** Histochemical staining of the bioprinted osteochondral interfaces for (a) Toluidine Blue, Alizarin Red, H&E, and OsteoImage, (b) IHC results for Coll2 and Osterix markers for both differentiation medium and miR transfection groups, (c) qRT-PCR gene expression results for osteogenic and chondrogenic gene markers at Week 4 (n = 3;  $p^* < 0.05$ ;  $p^{**} < 0.01$ ).

tissues formed by spheroids treated with osteogenic and chondrogenic differentiation medium exhibited higher expression levels for ACAN than bioprinted tissues formed by spheroids transfected with miR-148b and miR-(140 + 21). Even though the expression levels of osteogenic and chondrogenic markers, including BSP, OSTERIX, ACAN, were different for miR transfected and differentiation medium groups, the expression levels of SOX9, COL2A1, COL1A1, COL1, RUNX2, and BMP-4 were similar. The bioprinted constructs were analyzed as a whole (with both osteogenic and chondrogenic spheroids) while performing qRT-PCR, since spheroids merged at the end of four weeks. A hybrid medium (1:1 mixture of osteogenic and chondrogenic differentiation medium) was utilized for the bioprinted samples, which might cause cross-differentiation and affect the gene expression results.

#### 4. Discussions

Progenitor stem cells are promising tools for the situation where successful differentiation to native-like

chondrogenic and osteogenic tissues is required. The use of spheroids and their bioprinting have been investigated for the regeneration of cartilage and bone with different progenitor cell sources, including but not limited to adult mesenchymal stem cells (MSCs), ADSCs, and induced pluripotent stem cells [38, 39]. ADSCs, obtained from adipose tissue [40], have better proliferation rates than MSCs from bone marrow. In addition, the isolation of ADSCs follows an easy procedure with low tissue morbidity [41].

Scaffold-free approaches aim to mimic the native environment to promote the appropriate cell-cell interactions, leading to more natural differentiation, improved function and more robust tissue regeneration. The design of scaffold-free strategies for OLs is a promising avenue for development, but so far, few studies have demonstrated efficacy in clinical trials, such as the implantation of chondrospheres [42], likely due to the complexity of the OC interface. Although chondrospheres are promising candidates for restoring cartilage lesions, their use in OLs may pose limitations, such as the need for composite tissues for such lesions, necessitating a delicate

organization of chondrospheres in tandem with their osteogenic counterparts, which is not quite feasible using manual implantation strategies.

The use of miRs to modulate cell proliferation and differentiation in spheroids has the potential to overcome the limitations associated with the use of a differentiation medium with diffusible cytokines, which may cause ectopic tissue formation and disorganized tissue interfaces. Recent studies have shown that miRs play a critical role in cellular differentiation and proliferation in the human musculoskeletal system [21]. Our previous studies showed that a single dose of miR-148b can drive osteogenesis [43]. This study also demonstrated that transfection of miR-148b promoted osteogenesis in ADSC spheroids in agreement with previously published results [14, 15, 43]. Studies have also determined that miRs were closely associated with cell proliferation and regulation of cell cycles [13, 44]. Although a few studies showed that miR-148b inhibits cell proliferation in cancer cells by down-regulating TRIM59, which forms a part of the tripartite motif (TRIM) family [45], our results demonstrated that miR-148b promoted proliferation of ADSCs. The high proliferation rate can be related to the fact that miR-148b directly targets mitogenactivated protein kinase (MAPK) kinase 9 (MAP3K9) as discovered before [46]. In this study, our preliminary data showed that codelivery of miR-140 and -21 resulted in upregulated gene and increased protein expression compared to the delivery of each miR mimic alone. This strongly suggests the enhancement in chondrogenesis as a result of miR-21 and -140codelivery, at least within the time periods presented in this study. Previous studies with progenitor stem cells (MSCs and ADSCs) suggest that miR-21 is a strong modulator for ERK-MAPK signaling. ERK-MAPK signaling is the only active pathway in the osteogenic, chondrogenic, and adipogenic differentiation of stem cells [30, 31]. In addition, another study with ADSCs revealed that miR-21 promotes the differentiation by driving cells down a differentiation pathway with one post-transcriptional regulator and amplifying their differentiation effect [43]. In our study, miR-21 amplified the differentiation effect of miR-140 transfection as well as proliferation rate. The high proliferation rate can be related to the Wnt/ $\beta$ catenin signaling pathway as discovered before [47]. Both SOX9 and COL2A1 chondrogenic genes were significantly upregulated in the spheroids transfected by miR-(140 + 21) as compared to spheroids inducted with the differentiation medium at the end of third week, a common time-frame for chondrogenic differentiation. Interestingly, the ACAN gene was expressed well in transfected spheroids, in contrast to the chondrogenic spheroids inducted with the differentiation medium at Week 4, although ACAN is a weak late marker [48]. Gene expression, immuno and histochemical staining, and GAG biochemical assay

results showed improved differentiation for both spheroids transfected by miR-(140 + 21) and spheroids in the chondrogenic differentiation medium group. However, the transfected spheroids showed well preserved shapes as depicted in the H&E images, and high proliferation rate over time, even at Week 4. OC interfaces generated using the differentiation medium were prone to turn into a more spherical morphology when equal numbers of spheroids were bioprinted for each layer, such as in a  $3 \times 3$  configuration. To overcome this, first, we considered decreasing the gap between spheroids to prevent their possible displacement. Spheroids possess a spherical shape and the most efficient way of packing equalsize spheroids into a dual-layer interface is the facecentered cubic lattice [49] instead of placing them on top of each other. We preferred bioprinting in a 4 × 4 arrangement onto the cartilage zone and a  $3 \times 3$  arrangement onto the bone zone, rather than bioprinting both zones with the same configuration. Such an arrangement reduced the compaction of the OC interfaces with retained flat shape. This could be due to the fact that osteogenic spheroids possess a higher surface tension and hence less compaction compared chondrogenic spheroids [8], and providing a larger surface area for the chondrogenic zone with respect to the osteogenic zone initially might result in a similar total compaction for both

Although the effects of miR-148b and -140 on osteogenic and chondrogenic differentiation have been reported, respectively [15, 25], this study is the first demonstration of the combinatorial role of miR-140 and -21 on the chondrogenic differentiation of stem cells. Additionally, we investigated the induction potential of three miRs in a 3D spheroid model, rather than the conventionally used 2D approach. Importantly, we used miR-148b and miR-(140 + 21) together for the purpose of *in-situ* differentiation to create an OC interface. This innovative approach circumvents the limitations of the traditional medium recipe-dependent differentiation of stem cells into osteogenic and chondrogenic lineages. Therefore, the co-transfection of miR-140 and miR-21 is a novel alternative approach for chondrogenic induction methodology. This approach is promising for 3D bioprinting for regenerative medicine and cartilage tissue engineering as it has a high proliferation rate, even for differentiated mature cartilage cells, and a faster chondrogenic differentiation compared to the traditional approach. When osteogenic and chondrogenic spheroids were 3D bioprinted in a stratified heterotypic arrangement to mimic the native OC interface, spheroids further differentiated, demonstrating high levels of GAG and mineralization in the chondrogenic and osteogenic regions, respectively, and maintained the originally bioprinted bilayered morphology of the OC interface. Despite

that the presented work demonstrated the development of an OC interface, bioprinting has the capability to facilitate the scalable fabrication of OC tissues with the potential for reconstructing larger defects. For future work, we will target the generation of scalable OC tissues and test their efficacy in the reconstruction of OC defects *in vivo*. In sum, the capability of targeting damaged tissue via bioprinting and modulating osteogenic and chondrogenic differentiation provides a potential clinical approach for segmental bone and cartilage defects.

Although dual-layer heterotypic OC interfaces were bioprinted with tightly fused spheroids without delamination, the native OC tissue possesses a more complicated gradient heterogeneity. These gradient structures support smooth transition in mechanical properties, composition, and structure between the articular cartilage and subchondral bone. The bioprinted dual-layer OC interfaces also lack other crucial components present in vivo, such as enzymes, cytokines, and ECM proteins, which can facilitate the better recapitulation of native tissues. Also, the sample thickness may affect the differentiation and formation of the OC interface and thicker constructs can be ideal for transplantation studies. However, our goal in this work is to demonstrate an interface, which can be used for drug testing or disease modeling purposes. Therefore, a dual-layer structure with osteogenic spheroids in one zone and chondrogenic spheroids in the other zone was sufficient to check the crosstalk between zones for the formation of the OC interface.

In this study, we targeted the fabrication of an miR-induced scaffold-free OC interface, which can be used for drug testing or disease modeling (such as mucopolysaccharidosis type I disease) purposes. Such in-vitro models enable the analysis of molecular mechanisms and cellular interactions between chondrogenic and osteogenic zones. Understanding the crosstalk between chondrocytes and bone cells is essential when building and optimizing the structure of the interface between the strong, mechanoresistant bone component and the soft, load-spreading cartilage component [50]. However, the focus of OC interface research should be shifted from an approach solely considering cartilage or bone to an integrated approach based on the study of different components of the joint and their interactions, in order to better understand the mechanisms of the whole joint failure [51]. The presented OC interface can also be considered for *in-vivo* implantation after some major modifications. For example, OC interfaces should be built in greater thickness and maintained longer in vitro in order to improve the mechanical properties of bioprinted grafts before implantation.

The traditional differentiation method driven by diffusible cytokines is not a rapid differentiation method. Research on alternative methods revealed the need for miR transfection for differentiation purposes by regulating stem cell fate through targeting specific differentiation pathways. miR-148b was shown to upregulate BMPs by downregulating noggin (NOG), an antagonist of BMPs, with direct switching, miR-148b also induces ALP activity, an early biomarker of osteogenesis [52-55]. On the other hand, miR-140 was shown to upregulate SOX9 and Aggrecan proteins using the RALA target as explained before [25]. Although the mechanisms through osteogenesis and chondrogenesis via miRs were explained to some extent, more research is needed to clarify the detailed molecular mechanisms. However, it was shown that miRs transfection enabled more rapid and simple differentiation with a single-step procedure for yielding early maturation in a shorter culture period than those previously reported [56]. Our data also showed that miR transfection induced early-stage differentiation of ADSCs towards osteogenic and chondrogenic lineages, which is promising not only for modeling diseases in vitro using stem cells, but also for regenerative medicine applications.

#### 5. Conclusions

In this research, a 3D heterotypic tissue was bioprinted using spheroids of ADSCs transfected by miR-148b for the osteogenic layer and miR-(140 + 21) for the chondrogenic layer, and their potential for reconstructing the OC interface was evaluated. Our results showed that transfection of ADSC spheroids (a) induced chondrogenic differentiation by codelivery of miR-140 and miR-21, (b) induced osteogenic differentiation by miR-148b delivery, and (c) enabled the fabrication of OC interfaces with distinct osteogenic and chondrogenic layers with shape retention and enhanced cell proliferation. In sum, regulation of differentiation of stem cells with miR mimics is a promising tool for enhancing the control of tissue repair processes, particularly in OLs.

#### Data availability statement

All data that support the findings of this study are included within the article (and any supplementary files).

#### Acknowledgments

This work was supported by the National Institute of Dental and Craniofacial Research of the National Institutes of Health under Award Number RDE024790A (DJH), R01DE028614 (ITO), and the National Science Foundation Award Number 2033673 (DJH) and 1914885 (ITO). The authors thank R&D Systems (Minneapolis, MN) for providing several reagents. The opinions, interpretations,

conclusions, and recommendations are those of the author and are not necessarily endorsed by the National Institutes of Health or National Science Foundation.

#### Conflict of interest

I T O has an equity stake in Biolife4D and is a member of the scientific advisory board for Biolife4D and Brinter. Other authors confirm that there are no known conflicts of interest associated with this publication and there has been no significant financial support for this work that could have influenced its outcome.

#### ORCID iD

Ibrahim T Ozbolat https://orcid.org/0000-0001-8328-4528

#### References

- [1] Nooeaid P, Salih V, Beier J P and Boccaccini A R 2012 Osteochondral tissue engineering: scaffolds, stem cells and applications *J. Cell. Mol. Med.* **16** 2247–70
- [2] Mano J F and Reis R L 2007 Osteochondral defects: present situation and tissue engineering approaches J. Tissue Eng. Regen. Med. 1 261–73
- [3] Panseri S, Russo A, Cunha C, Bondi A, Di Martino A, Patella S and Kon E 2012 Osteochondral tissue engineering approaches for articular cartilage and subchondral bone regeneration *Knee Surg. Sports Traumatol. Arthrosc.* 20 1182–91
- [4] Jacob G, Shimomura K and Nakamura N 2020 Osteochondral injury, management and tissue engineering approaches Front. Cell Dev. Biol. 8 580868
- [5] Salgado C, Jordan O and Allémann E 2021 Osteoarthritis in vitro models: applications and implications in development of intra-articular drug delivery systems Pharmaceutics 13 60
- [6] Hutmacher D W 2001 Scaffold design and fabrication technologies for engineering tissues—state of the art and future perspectives J. Biomater. Sci. Polym. Ed. 12 107–24
- [7] Mironov V, Visconti R P, Kasyanov V, Forgacs G, Drake C J and Markwald R R 2009 Organ printing: tissue spheroids as building blocks *Biomaterials* 30 2164–74
- [8] Ayan B, Celik N, Zhang Z, Zhou K, Kim M H, Banerjee D, Wu Y, Costanzo F and Ozbolat I T 2020 Aspiration-assisted freeform bioprinting of pre-fabricated tissue spheroids in a yield-stress gel Commun. Phys. 3 1–14
- [9] Kim M H, Banerjee D, Celik N and Ozbolat I T 2022 Aspiration-assisted freeform bioprinting of mesenchymal stem cell spheroids within alginate microgels *Biofabrication* 14 024103
- [10] Ayan B, Wu Y, Karuppagounder V, Kamal F and Ozbolat I T 2020 Aspiration-assisted bioprinting of the osteochondral interface Sci. Rep. 10 1–12
- [11] Ratti M, Lampis A, Ghidini M, Salati M, Mirchev M B, Valeri N and Hahne J C 2020 MicroRNAs (miRNAs) and long non-coding RNAs (lncRNAs) as new tools for cancer therapy: first steps from bench to bedside *Target. Oncol.* 15 261–78
- [12] Yao S 2016 MicroRNA biogenesis and their functions in regulating stem cell potency and differentiation *Biol. Proced.* Online 18 1–10
- [13] Hwang H W and Mendell J T 2006 MicroRNAs in cell proliferation, cell death, and tumorigenesis Br. J. Cancer 94 776–80

- [14] Celik N, Kim M H, Hayes D J and Ozbolat I T 2021 miRNA induced co-differentiation and cross-talk of adipose tissue-derived progenitor cells for 3D heterotypic pre-vascularized bone formation *Biofabrication* 13 044107
- [15] Qureshi A T, Monroe W T, Dasa V, Gimble J M and Hayes D J 2013 miR-148b Nanoparticle conjugates for light mediated osteogenesis of human adipose stromal/stem cells *Biomaterials* 34 7799–810
- [16] Swingler T E et al 2012 The expression and function of microRNAs in chondrogenesis and osteoarthritis Arthritis Rheumatol. 64 1909–19
- [17] Zhang Y, Jia J, Yang S, Liu X, Ye S and Tian H 2014 MicroRNA-21 controls the development of osteoarthritis by targeting GDF-5 in chondrocytes Exp. Mol. Med. 46 e79
- [18] Ma S, Zhang A, Li X, Zhang S, Liu S, Zhao H, Wu S, Chen L, Ma C and Zhao H 2020 MiR-21-5p regulates extracellular matrix degradation and angiogenesis in TMJOA by targeting Spry1 Arthritis Res. Ther. 22 1–17
- [19] Seidl C I, Martinez-Sanchez A and Murphy C L 2016 Derepression of MicroRNA-138 contributes to loss of the human articular chondrocyte phenotype Arthritis Rheumatol. 68 398–409
- [20] Wang X B, Zhao F C, Yi L H, Tang J L, Zhu Z Y, Pang Y, Chen Y S, Li D Y, Guo K J and Zheng X 2019 MicroRNA-21-5p as a novel therapeutic target for osteoarthritis Rheumatology 58 1485–97
- [21] Mirzamohammadi F, Papaioannou G and Kobayashi T 2014 MicroRNAs in cartilage development, homeostasis, and disease Curr. Osteoporosis Rep. 12 410–9
- [22] McAlinden A, Varghese N, Wirthlin L and Chang L-W 2013 Differentially expressed microRNAs in chondrocytes from distinct regions of developing human cartilage PLoS One 8 e75012
- [23] Wienholds E, Kloosterman W P, Miska E, Alvarez-Saavedra E, Berezikov E, de Bruijn E, Horvitz H R, Kauppinen S and Plasterk R H A 2005 MicroRNA expression in zebrafish embryonic development *Science* 309 310–1
- [24] Tuddenham L, Wheeler G, Ntounia-Fousara S, Waters J, Hajihosseini M K, Clark I and Dalmay T 2006 The cartilage specific microRNA-140 targets histone deacetylase 4 in mouse cells FEBS Lett. 580 4214–7
- [25] Karlsen T A, Jakobsen R B, Mikkelsen T S and Brinchmann J E 2014 microRNA-140 targets RALA and regulates chondrogenic differentiation of human mesenchymal stem cells by translational enhancement of SOX9 and ACAN Stem Cells Dev. 23 290–304
- [26] Papaioannou G, Inloes J B, Nakamura Y, Paltrinieri E and Kobayashi T 2013 let-7 and miR-140 microRNAs coordinately regulate skeletal development *Proc. Natl Acad.* Sci. USA 110 E3291–300
- [27] Zhang J G, Wang J J, Zhao F, Liu Q, Jiang K and Yang G H 2010 MicroRNA-21 (miR-21) represses tumor suppressor PTEN and promotes growth and invasion in non-small cell lung cancer (NSCLC) Clin. Chim. Acta 411 846–52
- [28] Singh S K, Marisetty A, Sathyan P, Kagalwala M, Zhao Z and Majumder S 2015 REST—miR-21–SOX2 axis maintains pluripotency in E14Tg2a. 4 embryonic stem cells *Stem Cell Res.* 15 305–11
- [29] Kongcharoensombat W, Nakasa T, Ishikawa M, Nakamae A, Deie M, Adachi N, Mohamed A and Ochi M 2010 The effect of microRNA-21 on proliferation and matrix synthesis of chondrocytes embedded in atelocollagen gel *Knee Surg.* Sports Traumatol. Arthrosc. 18 1679–84
- [30] Mei Y, Bian C, Li J, Du Z, Zhou H, Yang Z and Zhao R C H 2013 miR-21 modulates the ERK-MAPK signaling pathway by regulating SPRY2 expression during human mesenchymal stem cell differentiation J. Cell. Biochem. 114 1374–84
- [31] Chen J, Deng S, Zhang S, Chen Z, Wu S, Cai X, Yang X, Guo B and Peng Q 2014 The role of miRNAs in the differentiation of adipose-derived stem cells *Curr. Stem Cell Res. Ther.* 9 268–79
- [32] Mohamed-Ahmed S, Fristad I, Lie S A, Suliman S, Mustafa K, Vindenes H and Idris S B 2018 Adipose-derived

- and bone marrow mesenchymal stem cells: a donor-matched comparison *Stem Cell Res. Ther.* **9** 1–15
- [33] Catelas I, Sese N, Wu B M, Dunn J C Y, Helgerson S and Tawil B 2006 Human mesenchymal stem cell proliferation and osteogenic differentiation in fibrin gels *in vitro Tissue Eng.* 12 2385–96
- [34] Glueck M, Gardner O, Czekanska E, Alini M, Stoddart M J, Salzmann G M and Schmal H 2015 Induction of osteogenic differentiation in human mesenchymal stem cells by crosstalk with osteoblasts *Biores. Open Access* 4 121–30
- [35] Ayan B, Heo D N, Zhang Z, Dey M, Povilianskas A, Drapaca C and Ozbolat I T 2020 Aspiration-assisted bioprinting for precise positioning of biologics Sci. Adv. 6 eaaw5111
- [36] Moncal K K et al 2021 Intra-operative bioprinting of hard, soft, and hard/soft composite tissues for craniomaxillofacial reconstruction Adv. Funct. Mater. 31 2010858
- [37] Akkouch A, Yu Y and Ozbolat I T 2015 Microfabrication of scaffold-free tissue strands for three-dimensional tissue engineering *Biofabrication* 7 031002
- [38] Leberfinger A N, Ravnic D J, Dhawan A and Ozbolat I T 2017 Concise review: bioprinting of stem cells for transplantable tissue fabrication Stem Cells Transl. Med. 6 1940–8
- [39] Datta P, Dhawan A, Yu Y, Hayes D, Gudapati H and Ozbolat I T 2017 Bioprinting of osteochondral tissues: a perspective on current gaps and future trends *Int. J. Bioprinting* 3 111
- [40] Wu Y, Ayan B, Moncal K K, Kang Y, Dhawan A, Koduru S V, Ravnic D J, Kamal F and Ozbolat I T 2020 Hybrid bioprinting of zonally stratified human articular cartilage using scaffold-free tissue strands as building blocks Adv. Healthcare Mater. 9 2001657
- [41] Zhou L N, Wang J C, Zilundu P L M, Wang Y Q, Guo W P, Zhang S X, Luo H, Zhou J H, Deng R D and Chen D F 2020 A comparison of the use of adipose-derived and bone marrow-derived stem cells for peripheral nerve regeneration in vitro and in vivo Stem Cell Res. Ther. 11 1–16
- [42] Armoiry X, Cummins E, Connock M, Metcalfe A, Royle P, Johnston R, Rodrigues J, Waugh N and Mistry H 2019 Autologous chondrocyte implantation with chondrosphere for treating articular cartilage defects in the knee: an evidence review group perspective of a NICE single technology appraisal *Pharmacoeconomics* 37 879–86
- [43] Abu-Laban M et al 2019 Combinatorial delivery of miRNA-nanoparticle conjugates in human adipose stem cells for amplified osteogenesis Small 15 1902864

- [44] Bueno M J and Malumbres M 2011 MicroRNAs and the cell cycle Biochim. Biophys. Acta 1812 592–601
- [45] Yuan L, Liu Y, Qu Y, Liu L and Li H 2019 Exosomes derived from MicroRNA-148b-3p-overexpressing human umbilical cord mesenchymal stem cells restrain breast cancer progression Front. Oncol. 9 1076
- [46] Nie F et al 2016 MicroRNA-148b enhances proliferation and apoptosis in human renal cancer cells via directly targeting MAP3K9 Mol. Med. Rep. 13 83–90
- [47] Zhang W-M, Zhang Z-R, Yang X-T, Zhang Y-G and Gao Y-S 2018 Overexpression of miR21 promotes neural stem cell proliferation and neural differentiation via the Wnt/βcatenin signaling pathway in vitro Mol. Med. Rep. 17 330–5
- [48] Mwale F, Stachura D, Roughley P and Antoniou J 2006 Limitations of using aggrecan and type X collagen as markers of chondrogenesis in mesenchymal stem cell differentiation J. Orthop. Res. 24 1791–8
- [49] Hales T C 2011 Historical overview of the Kepler conjecture The Kepler Conjecture (New York: Springer) pp 65–82
- [50] Thysen S, Luyten F P and Lories R J U 2015 Targets, models and challenges in osteoarthritis research Dis. Models Mech. 8 17–30
- [51] Wei W and Dai H 2021 Articular cartilage and osteochondral tissue engineering techniques: recent advances and challenges *Bioact. Mater.* 6 4830–55
- [52] Chang Y H and Hu Y C 2017 Improved calvarial bone repair by hASCs engineered with Cre/loxP-based baculovirus conferring prolonged BMP-2 and MiR-148b co-expression J. Tissue Eng. Regen. Med. 11 3068–77
- [53] Canalis E, Economides A N and Gazzerro E 2003 Bone morphogenetic proteins, their antagonists, and the skeleton Endocr. Rev. 24 218–35
- [54] Schoolmeesters A, Eklund T, Leake D, Vermeulen A, Smith Q, Aldred S F and Fedorov Y 2009 Functional profiling reveals critical role for miRNA in differentiation of human mesenchymal stem cells PLoS One 4 9
- [55] Mollazadeh S, Fazly Bazzaz B S, Neshati V, de Vries A A F, Naderi-Meshkin H, Mojarad M, Mirahmadi M, Neshati Z and Kerachian M A 2019 Overexpression of MicroRNA-148b-3p stimulates osteogenesis of human bone marrow-derived mesenchymal stem cells: the role of MicroRNA-148b-3p in osteogenesis BMC Med. Genet. 20 1–10
- [56] Ishikawa M et al 2020 miRNA-based rapid differentiation of purified neurons from hPSCs advancestowards quick screening for neuronal disease phenotypes in vitro Cells 9 532